Effects of Injection Location, Flow Ratio and Geometry on Kenics Mixer Performance

D. M. Hobbs and F. J. Muzzio
Dept. of Chemical and Biochemical Engineering, Rutgers University, Piscataway, NJ 08855

The performance of the Kenics static mixer for mixing small streams of passive tracer into the bulk flow is investigated as a function of injection location and flow ratio. Flow ratios of 1/99 and 10/90 are simulated at nine different injection locations, and two alternative geometries are considered in addition to the standard Kenics mixer. Mixing is evaluated qualitatively by examining the spread of the tracer on cross-sectional slices from the mixer and quantitatively by computing the variation coefficient as a function of axial position. For the standard Kenics geometry, injection location strongly affects the extent of mixing only for the first few elements, after which the mixing rate is independent of injection location. In a sufficiently long mixer, material injected at any location spreads to the entire flow, but the least effective injection locations require up to four elements more than the most effective locations to achieve the same variation coefficient. A faster rate of decrease in variation coefficient is observed for a flow ratio of 1/99 vs. 10/90. An alternative geometry in which the elements have 120° of twist instead of the standard 180° of twist shows a similar dependence on injection location and flow ratio, but is more energy-efficient than the standard Kenics geometry. In another alternative geometry in which all elements have the same direction of twist, segregated islands exist in the flow. For injection locations inside the segregated islands, virtually no mixing takes place; for injection locations outside of the segregated islands, the tracer spreads to the remaining flow but does not penetrate the islands.

Introduction

Fluid mixing has a distinct impact on the outcome of many industrial processes, including both simple blending and more complex operations where mixing is coupled with other processes such as crystallization, oxygen transfer to cell cultures, and rapid chemical reactions. One industrial mixing device that is used in a variety of applications from polymer processing (Middleman, 1977) to biotechnology (Paul, 1990) is the static mixer. However, despite widespread use, the mixing performance in static mixers is typically not well characterized. As a first step, it is often difficult to obtain detailed information about the velocity fields in industrial systems. Once the velocity field is known, it is generally even more difficult to use the information contained in the velocity field to obtain a useful quantitative description of mixing in the system. The complex, 3-dimensional geometries and flow fields typical of most static mixers make analytic solutions of the velocity field in such equipment impractical. However, for laminar flows, a high-quality numerical solution of the velocity field can provide a starting point to characterize mixing performance.

Recently, this approach was successfully employed to analyze an industrial mixing device: the Kenics static mixer, manufactured by Chemineer (Dayton, OH). Computational fluid dynamics (CFD) was used to obtain the velocity field for the flow. Previous communications described the use of this technique to analyze the flow and mixing in the Kenics mixer (Hobbs and Muzzio, 1997a,b; Hobbs et al., 1997a). The CFD-generated velocity field was used as input to software that tracks the motion of fluid tracers in the flow. Other properties of interest, such as the deformation tensor and the evolution of the stretching of fluid filaments, were computed. Good agreement was achieved between computational results and experimental data for pressure drop (Hobbs and Muzzio, 1997a), striation development, residence time distri-

Correspondence concerning this article should be addressed to F. J. Muzzio.

butions, variation coefficient (Hobbs and Muzzio, 1997b), and a tracer mixing study (Hobbs et al., 1997a). The close correspondence between computations and experiments served to validate the simulation results and indicated that the simulations provided a good model of the physical system.

One frequently encountered industrial application for static mixers is blending a small quantity of a minor component into a larger stream of the major component. Examples of this type of operation include mixing a small amount of colorant into a bulk polymer or mixing a concentrated stream of one reagent into a more dilute stream containing a second reagent. The potential effect of poor mixing in such situations ranges from nonuniform product appearance to overproduction of impurities from competing chemical reactions. For mixing operations of this type, two practical considerations are the effect of injection position and the effect of the flow ratio of injected material to the total flow on mixing performance. This article seeks to address these issues for the Kenics mixer by employing the combination of CFD and tracking techniques described earlier to simulate mixing a small quantity of tracer into the bulk flow. Qualitative results of the tracer tracking simulations are presented by examining the partially mixed structures generated by the tracer on representative cross-sectional slices from the mixer. Mixing performance is quantified using the variation coefficient ($\sigma/\bar{N}$). A previous communication (Hobbs and Muzzio, 1997b) described the use of CFD and tracer tracking computations to generate variation coefficient results for the standard Kenics mixer that agreed very well with the available experimental data (Allocca, 1982; Pahl and Muschelknautz, 1982). The previous experimental and computational results considered a single mixing scenario: a 10% injection of tracer introduced along the mixer center line. In this article, other mixing configurations are considered, including nine different injection locations, 1% and 10% tracer injections, and three different mixer geometries. For each system, the variation coefficient is computed as a function of mixer length to quantify mixing performance.

The remainder of this article is organized as follows. The second section briefly describes the methods used to obtain the velocity field in the Kenics mixer, to carry out tracer tracking simulations, and to compute the variation coefficient as a function of position. The third section presents a discussion of results for various injection locations, tracer flow ratios, and mixer geometries. Finally, the fourth section summarizes the conclusions of this work.

Methods

Velocity field

The mixer configuration chosen as a base case was a Kenics mixer with open tube entrance and exit sections (Figure 1). In the standard Kenics configuration, each element of the mixer is a plate that has been given a 180° helical twist. The complete mixer consists of a series of elements of alternating clockwise and counterclockwise twist arranged axially within a pipe so that the leading edge of an element is at right angles to the trailing edge of the previous element. Details of the system geometry and fluid properties used in the CFD computations are given in Table 1. The inlet velocity adopted in the base case simulation is $\langle v_x \rangle = 0.0012$ m/s, giving an open tube Reynolds number [$\mathrm{Re} = (\rho \langle v_x \rangle D/\mu)$] of 0.15. Numerical results show that for this low Reynolds number, the flow is well inside the creeping, reversible regime (Hobbs and Muzzio, 1997a). A commercially available CFD software package (FLUENT/UNS) was used to obtain the velocity field in the static mixer. A full discussion of the grid generation, grid validation, and solution procedure using this software was previously presented (Hobbs and Muzzio, 1997a).

Table 1. Mixer Geometry and Fluid Properties

Mixer	
Diameter (D)	5.08 cm
Plate thickness	0.3175 cm
Entrance length	10.16 cm
Exit length	10.16 cm
Fluid	
Density (ρ)	1.20 g/cm^3
Viscosity (μ)	500 cp

In addition to the standard Kenics geometry, two variations on the Kenics geometry were also investigated. The first is an alternative geometry in which all elements have righthanded twist. In this case, there are poorly mixed regions in the flow that do not exchange material with the remainder of the system (Hobbs et al., 1997b). While this alternative geometry is not a practical substitute for the standard Kenics mixer (at least for the majority of mixing applications, in which global homogeneity is the goal), it does provide an interesting case study due to the presence of coexisting regions of good and poor mixing. The second variation is a Kenics mixer in which each element has 120° of twist, as opposed to the standard 180° of twist. Computations of mixer efficiency (in terms of stretching rate normalized by energy input) have shown that the 120° twist configuration is roughly 40% more energy efficient than the standard 180° twist Kenics configuration. This system is of practical interest since it provides a means of achieving equivalent mixing performance for a significantly reduced energy expenditure.

For the remainder of this article, the three different mixer geometries are denoted as follows: standard Kenics geometry = 180° R-L; alternative geometry in which all elements have righthanded twist = 180° R-R; alternative geometry with 120° twisted elements = 120° R-L. A separate geometry and grid were created for each of the mixer configurations. CFD computations were performed for the two alternative geometries as well as the standard Kenics configuration to obtain velocity fields for each system. These velocity fields served as a

Figure 1. Six-element Kenics static mixer in the standard 180° R-L configuration.

starting point for further characterization of the mixer performance through the use of the tracking techniques that are described next.

Tracking computations

Computer software was developed to track fluid tracers as they move through the mixer flow field, using the CFD-generated velocity field as input. Trajectories are tracked by integrating the vector equation of motion

$$\frac{dx}{dt} = v(x) \tag{1}$$

for each tracer using a fourth-order Runge-Kutta integration scheme with adaptive step-size control (Press et al., 1986). For the low Reynolds number flow considered here, the Kenics velocity field shows a periodicity matching that of the mixer geometry (Fan et al., 1970). The particle-tracking software takes advantage of this periodicity to extend the simulation results from a six-element mixer to devices of greater length. The six-element base case is divided into an entrance section (inlet tube and first two Kenics elements), exit section (outlet tube and Kenics element 5 and 6), and central periodic section (Kenics elements 3 and 4). Within the particle-tracking software, the central section is repeated as a spatially periodic unit to extend the tracking to a mixer of any length.

For each geometry just described, tracking computations were performed to simulate the mixing of passive tracers. Nine injection locations were chosen near the inlet to the mixer, with each injection located axially 0.1 cm upstream from the leading edge of the first mixer element. The cross-sectional positions of the centers of each injection location (*a* through *i*) are shown in Figure 2a. The Kenics geometry has a reflexive symmetry with respect to the central axis; therefore, the chosen injection locations are analogous to injection locations located at corresponding positions in the lower half of the mixer cross section. Tracking computations were performed to simulate either a 1 vol. % injection of tracer or a 10 vol. % injection of tracer at each injection location. For each simulation, ~10,000 tracers were placed into the flow at the injection point. The spacing of the tracers was adjusted for each case, so that the tracers covered a flow region corresponding to the appropriate fraction of the flow (for example, Figure 2b shows the tracer injection profile for a 1% tracer injection at each location in the 180° R – L flow). The tracers were tracked through the flow by integration of Eq. 1, and at each periodic plane (i.e., the planes after the second Kenics element, fourth element, sixth element, etc.) the positions were recorded. The tracking of 10,000 tracers through a 16-element Kenics mixer in the standard 180° R-L configuration required 135 Mb of RAM and approximately 53 h of CPU time on a Sun hyperSPARC 20/712 workstation. From each of the tracer tracking computations, results were obtained for tracer positions at each periodic plane and used to compute the variation coefficient, as described in the next section.

Variation coefficient

Building on the intensity of segregation concept from Danckwerts (1952), mixture quality has often been quantified in terms of a mixing index that describes the degree of homogeneity of the system. (Fan et al., 1970 describe over thirty indices of this type.) The mixture homogeneity is evaluated based on a statistical analysis of samples from the mixture, and typically the mixing index is expressed as a function of the standard deviation (σ) or variance (σ^2) of the mixture samples, where the mixture variance is defined as

$$\sigma^2 = \frac{\sum_{i=1}^{n} (C_i - \bar{C})^2}{n-1}, \tag{2}$$

where C_i is the concentration of the ith sample, $\bar{C}$ is the mean value of concentration, and n is the number of samples. For the Kenics static mixer, experimental data for mixture quality has previously been reported in terms of the variation coefficient, $\sigma/\bar{C}$ (Allocca, 1982; Pahl and Muschelknautz, 1982), also known as the relative standard deviation (RSD). Although some properties of interest for a continuous-flow system are more properly described when weighted based on volumetric flow rate (e.g., the residence time distribution (Nauman, 1991), the typical experimental approach for variation coefficient weights all measurements on a planar cross section equally. Therefore, this equally weighted approach was adopted here.

Due to the discrete nature of the tracer-tracking results, a number-based variation coefficient $\sigma/\bar{N}$ was used as a measure of mixture homogeneity. The number-based variation coefficient for a given mixer cross section was calculated as follows. A square grid of 64×64 cells was laid out to cover the mixer cross section. Cells that fall entirely within the flow domain were retained for calculation purposes, while cells that fall partially or completely outside of the flow domain were discarded. A total of $n = 2{,}600$ cells were retained. Based on the locations of the tracer particles on the mixer cross-section, the number of tracers in each cell (N_i) and the total number of particles that fall within the cells (N_{tot}) were computed. The average number of tracers per cell was computed as $\bar{N} = N_{\text{tot}}/n$, and the variance σ_N^2 was computed via Eq. 2 with N_i in place of C_i and $\bar{N}$ in place of $\bar{C}$ to obtain the number-based variation coefficient $\sqrt{\sigma_N^2}/\bar{N} = \sigma/\bar{N}$. For each of the geometries and tracer-injection locations described earlier, the variation coefficient was computed for each periodic mixer cross section. The following section presents results from the tracer-tracking and variation coefficient computations for each case.

Results and Discussion

Tracer mixing

The first case considered was the standard industrial Kenics mixer in the 180° R-L configuration. Tracking experiments were performed for a 1% tracer injection at each of the injection points shown in Figure 2a. Figures 3, 4 and 5 show the cross-sectional profiles obtained after 2, 6 and 12 elements, respectively, for tracer starting at each injection location. After 2 elements (Figure 3), very little mixing has taken place and the tracer is still confined to a very small portion of the flow. At this point, the structure of the striation pattern is quite sensitive to injection location. After a few more ele-

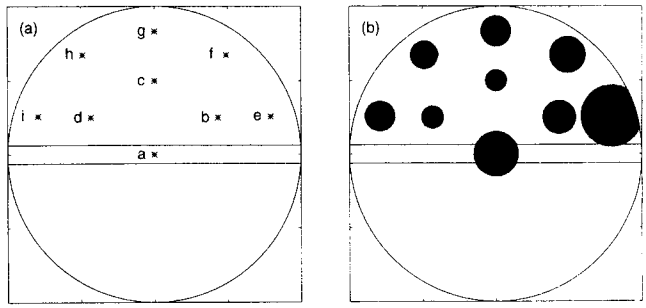

Figure 2. Tracer injection: (a) cross section (0.1 cm upstream of the leading edge of the first mixer element) and the edge of the mixer; (b) 1 vol. % injection of tracer at each location in the 180° R-L case.

ments (Figure 4), more complicated striation patterns have developed. While differences are still readily apparent in the structures achieved from each injection position, a general similarity of the partially mixed structures has become evident. The evolution of the tracer structures illustrates the mechanisms that contribute to mixing in the Kenics mixer: the initial circular injection of points is stretched into a ribbon, which is elongated, reoriented, and folded by the flow within individual elements, and cut by the leading edges of sequential mixer elements. After 12 elements (Figure 5), differences in the tracer structures are minimal. In each case, the tracer has spread to essentially all of the flow domain.

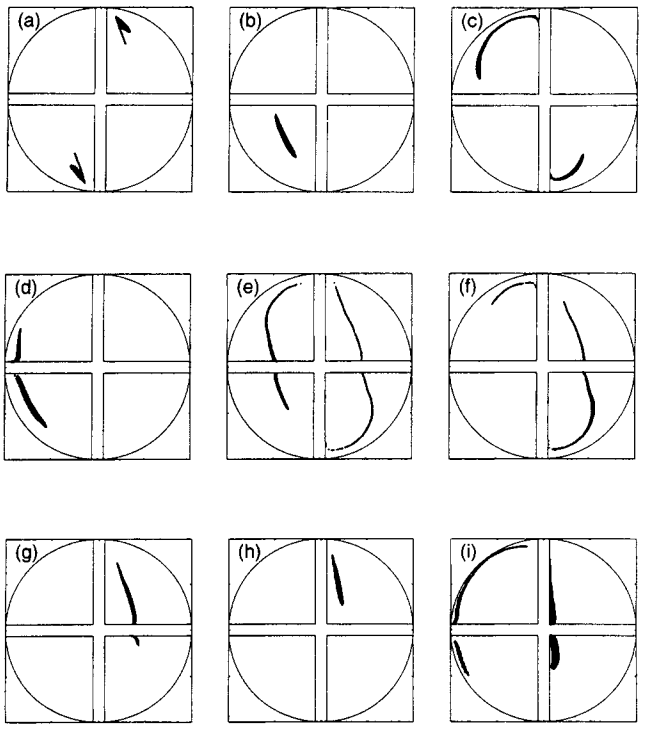

Figure 3. Cross-sectional profiles for 1% tracer mixing in a Kenics mixer in the standard 180° R-L configuration after 2 elements for each injection location in Figure 2a.

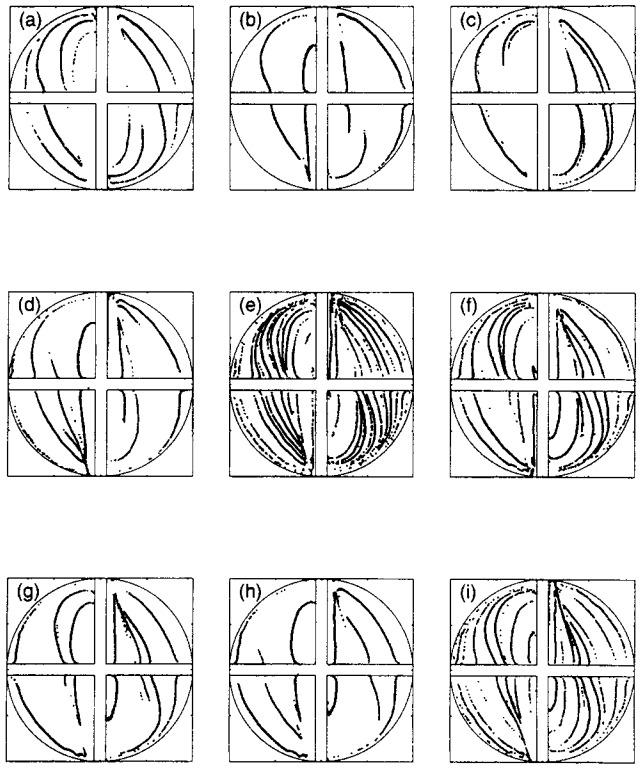

Figure 4. Cross-sectional profiles for 1% tracer mixing in a Kenics mixer in the standard 180° R-L configuration after 6 elements for each injection location in Figure 2a.

A similar set of tracking computations was performed for a 10% tracer injection at each of the nine locations in the 180° R-L case. Cross sections from each of these experiments after 2, 6 and 12 elements are shown in Figures 6, 7 and 8, respectively. The 10% tracer results reveal a similar trend to the 1% tracer case: a strong dependence on injection location is evident initially (Figure 6), but similar structures begin to appear after a few elements (Figure 7), and essentially no difference in the tracer patterns is evident after 12 elements (Figure 8). This independence of initial conditions is an intrinsic property of globally chaotic flows and has been observed in experiments and simulations (Leong and Ottino, 1989; Swanson and Ottino, 1990). Previous analysis of the standard Kenics mixer has suggested that the flow in this device is globally chaotic (Hobbs and Muzzio, 1997b). One of the defining features of a chaotic system is that any tracer located inside the chaotic region will sample the entire chaotic region as the number of periods becomes infinite. As the number of mixer elements is increased, differences between injection positions in the chaotic region become less important to the extent of mixedness in the system.

From Figures 4 and 7, it is evident that certain injection positions lead to better tracer dispersion over the first few mixer elements for both 1% and 10% tracer injections. Injection location *e* provides the best mixing performance, and locations *f* and *i* provide somewhat better mixing than the remaining injection points. The question of why certain injection locations lead to better initial mixing performance can be answered using techniques from dynamical systems theory

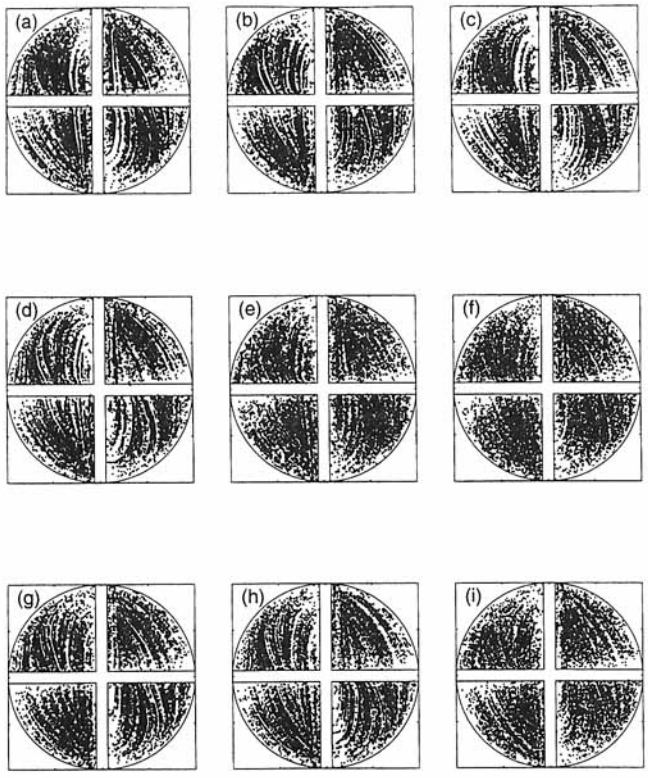

Figure 5. Cross-sectional profiles for 1% tracer mixing in a Kenics mixer in the standard 180° R-L configuration after 12 elements for each injection location in Figure 2a.

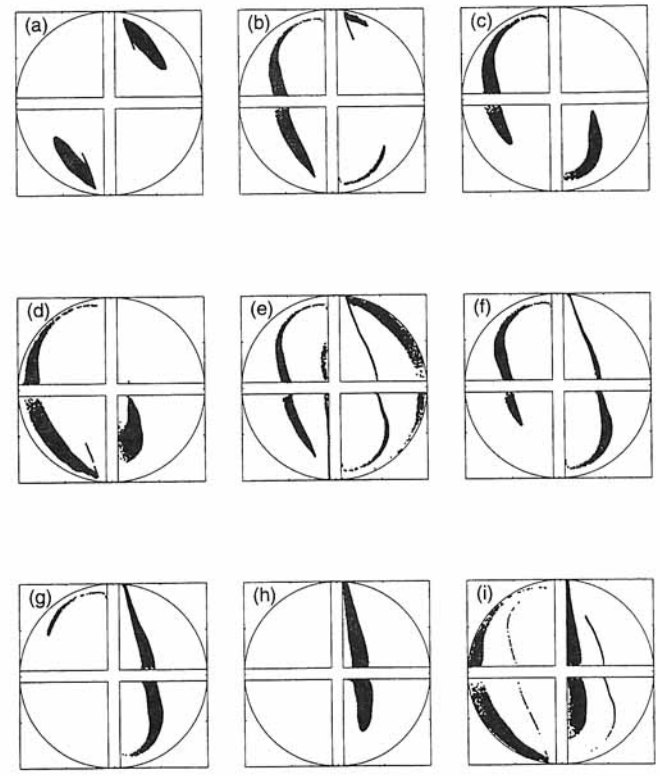

Figure 6. Cross-sectional profiles for 10% tracer mixing in a Kenics mixer in the standard 180° R-L configuration after 2 elements for each injection location in Figure 2a.

to analyze the chaotic flow in the Kenics mixer. A previous study computed the stretching of vector elements along tracer trajectories in the 180° R-L Kenics flow (Hobbs and Muzzio, 1997b). The amount of intermaterial surface generated in a region of the flow is directly proportional to the amount of stretching experienced by material elements in that region. The rate of stretching determines the rate of the micromixing process both by increasing the intermaterial area over which interdiffusion of components can occur, and also by decreasing the required diffusional distance. The positions of points experiencing high and low stretching correspond to regions of good and poor micromixing, respectively. Regions of high stretching in chaotic flows are typically associated with hyperbolic periodic points in the flow, which have stable and unstable manifolds along which fluid elements approach and leave the points, respectively. Fluid that passes close to the hyperbolic periodic point will be subjected to a high amount of stretching. For the 180° R-L flow, two period-1 hyperbolic points are located symmetrically in the cross-sectional plane between periodic segments near the upper right and lower left corners of the vertical element edge; the manifold structures for the two periodic points are also symmetric (Hobbs and Muzzio, 1997b). Tracer injection locations *e*, *f*, and *i* lie along the stable manifolds in locations where the fluid will pass close to the periodic points within one period (two elements). Fluid injected at these locations will be stretched more intensely as it passes through the first mixer elements, and the initial tracer dispersion will be better than for fluid injected at other locations.

The overall similarity of the partially mixed structures generated for the different injection locations can also be explained in terms of the manifolds of the hyperbolic points. The dominant feature of the unstable manifold of the period-1 point in quadrant 1 is a streak that emanates from the point and stretches down and to the right cross the flow cross section. For a higher number of periods, the unstable manifold structure develops branches that fan off from the initial streak (Hobbs and Muzzio, 1997b). The self-similar striation patterns that develop for all tracer injection locations in Figures 3–8 closely follow the structure of the unstable manifolds. The complete manifold for the periodic point is an invariant structure (i.e., the structure of the manifold is the same when examined at periodic intervals) and has infinite length. After a sufficient number of periods, trajectories that start inside the chaotic region of the flow will asymptotically approach all points within the chaotic region. Therefore, the performance of all injection locations becomes similar as the number of mixer elements increases.

The second geometry considered was the 180° R-R case in which all mixer elements have righthanded twist. (It should be noted that the choice of righthanded elements is arbitrary and that a mixer geometry with lefthanded elements would behave exactly as a mirror image of the 180° R-R case due to symmetry). Previous investigation of this mixer geometry (Hobbs and Muzzio, 1997a,b) has demonstrated that in this configuration, segregated regular regions exist that do not exchange material with the remaining chaotic portion of the flow. The positions of these segregated regions in the mixer

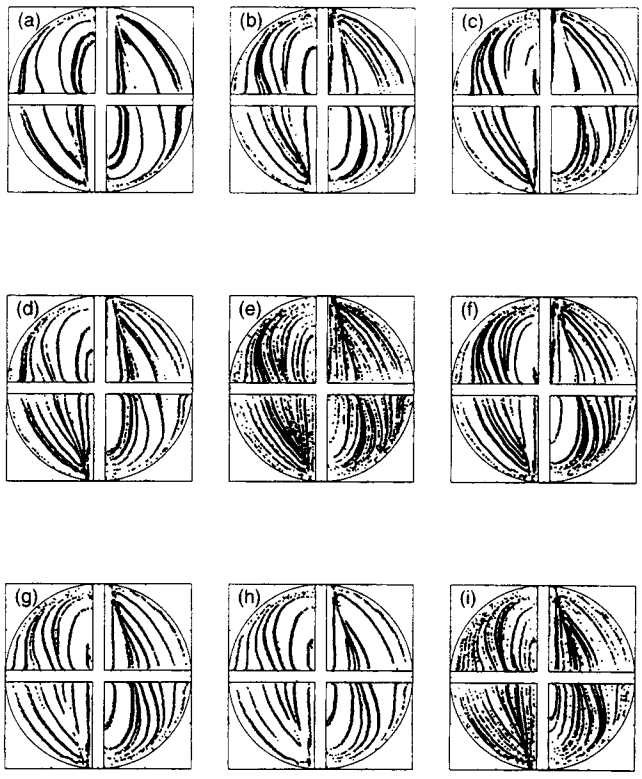

Figure 7. Cross-sectional profiles for 10% tracer mixing in a Kenics mixer in the standard 180° R-L configuration after 6 elements for each injection location in Figure 2a.

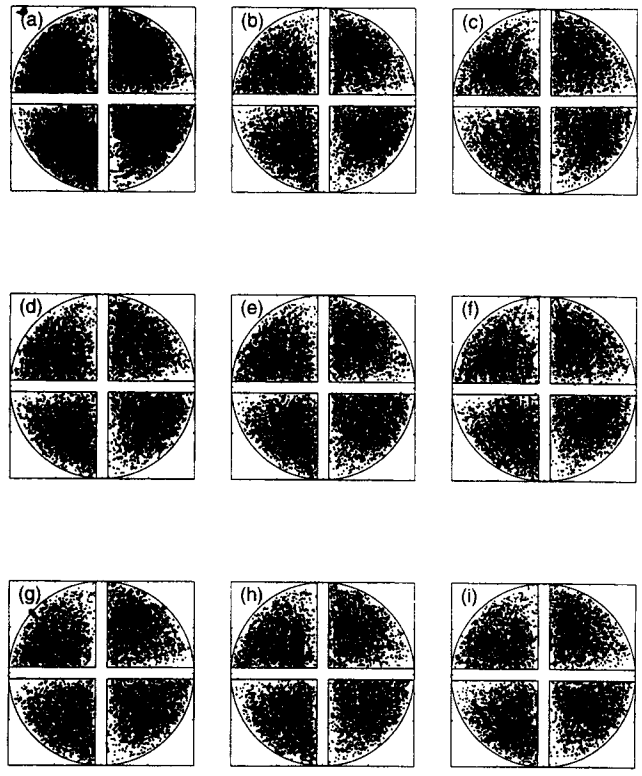

Figure 8. Cross-sectional profiles for 10% tracer mixing in a Kenics mixer in the standard 180° R-L configuration after 12 elements for each injection location in Figure 2a.

cross section at the periodic plane after 2, 4, 6, ... mixer elements are shown in Figure 9. For the 180° R-R geometry, tracking experiments were performed for a 1% tracer injection at each of the nine injection points shown in Figure 2a. Cross sections from each of these experiments after 2, 6 and 12 elements are shown in Figures 10, 11 and 12, respectively. For this case, the distinct differences in tracer behavior with respect to injection location are evident. For injections that fall entirely within the chaotic region of the flow (positions *a*, *b*, *e* and *f*), the tracer behaves similarly to the 180° R-L case: the partially mixed structures have an initial dependence on injection location, but the tracer spreads to the entire chaotic region of the flow after a sufficient number of elements. In this case, however, the tracer still never penetrates the segregated islands, even after a large number of elements. Other injection locations fall entirely within the regular regions of the flow (positions *g*, *h*, and *i*). In this case, the tracer remains inside the regular regions regardless of the number of mixer elements. The tracer spreads very slowly inside the regular regions, and does not spread at all into the chaotic portions of the flow. Finally, some of the injection locations (*c* and *d*) fall on the boundary between the chaotic and regular flow zones. In this case, a portion of the tracer spreads to cover the chaotic flow region while the remainder is trapped in the regular flow domain.

The third mixer geometry investigated was 120° R-L configuration. Previous computations demonstrated that this mixer geometry is more energy efficient than the standard Kenics configuration and produces mixtures of equivalent quality in shorter mixers with significantly smaller pressure drop (Hobbs et al., 1997b). Therefore, this configuration was chosen for further investigation by tracer mixing studies. Tracking experiments were performed for tracer injection at each of the injection points shown in Figure 2a. Figures 13, 14 and 15 show the cross-sectional profiles obtained after 2, 6 and 12 elements, respectively, for a 1% tracer injection at each introduction point, and Figs. 16, 17 and 18 show results at corresponding locations for a 10% tracer injection. In the 120° R-L geometry, the flow is also globally chaotic, and results for this case closely parallel those for the 180° R-L geometry. Again, differences in injection position manifest themselves only over the first few elements (Figures 13, 14, 16 and 17), but are essentially erased as the number of elements is increased (Figures 15 and 18. The stable and unstable manifolds for this geometry have a similar structure to the 180° R-L case, with the locations of the hyperbolic points rotated slightly clockwise in the 120° R-L case.

While the evolution of striation patterns provides a useful qualitative understanding of the progress of fluid mixing within the static mixer, a quantitative description of the mixture quality provides a more practical means of evaluating mixer performance. In the next subsection, the variation coefficient is used as a quantitative measure of mixing performance for the different mixing scenarios considered thus far.

Variation coefficient

The tracer mixing computations shown in the previous sec-

tion provide the position of the tracers on each periodic plane in the static mixer (i.e., the planes after the second element, fourth element, sixth element, etc.). For each mixer cross section, the variation coefficient was computed as described in the previous subsection on the variation coefficient. The number-based variation coefficient was plotted as a function of axial position in the mixer and used as a basis of comparison among different mixing conditions.

The results for the variation coefficient vs. the normalized axial position X are shown in Figure 19a for 1% tracer injections in the 180° R-L geometry. For each injection location the calculated variation coefficient decreases monotonically from the inlet of the mixer up to $X \approx 15$ (10 mixer elements). After this point, the variation coefficient levels out, indicating that the characteristic length for the mixture has fallen below the scale of the grid size used for calculation, and further homogenization of the mixture cannot be determined at this level of resolution. Increasing the resolution of the variation coefficient by two mixer elements would require a sixteenfold increase in the number of tracked particles, and a corresponding increase in the computation time (to approximately 900 h of CPU time on a Sun SPARC 20/712). However, since the effects of the initial conditions are erased in about six elements, the variation coefficient data for the first 10 mixer elements is sufficient for further calculations and the marginal increase in resolution that could be obtained with more extensive computations does not justify the increase in computational time.

The set of tracer injection points produces a family of variation coefficient curves in Figure 19a. In all nine cases, the variation coefficient decreases exponentially with progress through the mixer. The exponential reduction in variation coefficient can be correlated by an equation of the form:

$$\frac{\sigma}{\overline{N}} = A \exp(-BX), \tag{4}$$

which is frequently used to describe data of this type (Godfrey, 1992). The coefficient B represents the rate of decrease in the variation coefficient per unit mixer length. For the nine injection locations, the variation coefficient vs. position curves have similar B values, ranging from 0.154 to 0.177, with an average $\overline{B}$ of 0.167. This indicates that all injection locations lead to a similar rate of reduction in variation coefficient with respect to mixer length.

Variation coefficient results for a 10% tracer injection at each injection location in the 180° R-L geometry are shown in Figure 19b. Essentially parallel curves are again obtained for each injection location up to $X = 15$. The starting value for the 10% curves in Figure 19b is lower than for the 1% curves in Figure 19a, since a greater portion of the flow cross section initially contains tracer. The rate of reduction in variation coefficient is slower for the 10% tracer injection; $\overline{B}$ for the 10% case is 0.116 vs. 0.167 for the 1% case. The simulations for both tracer quantities indicate that all injection locations in the 180° R-L mixer give approximately the same rate of reduction of variation coefficient. This implies that whatever injection location is chosen, the desired extent of mixing can be achieved, given a sufficient number of elements. However, from the results in Figure 19a and 19b (and

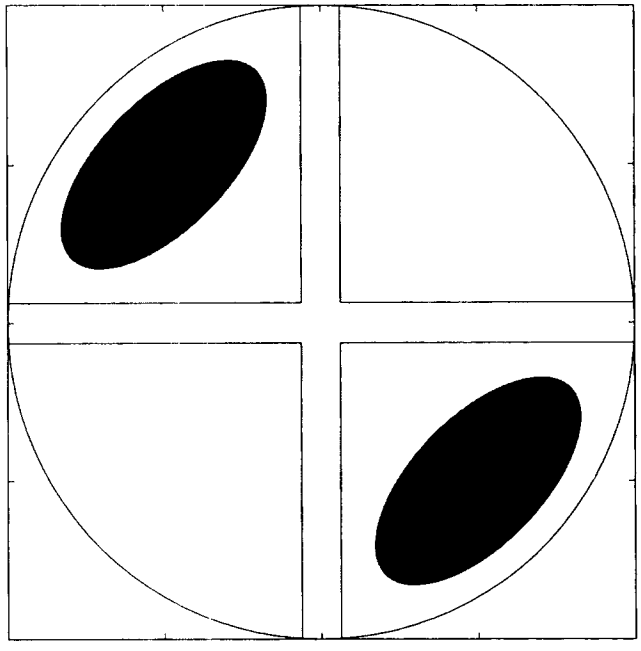

Figure 9. Location of segregated regions in the periodic planes after 2, 4, 6, ... mixer elements in the alternate Kenics geometry where all elements have the same direction of twist (180° R-R case).

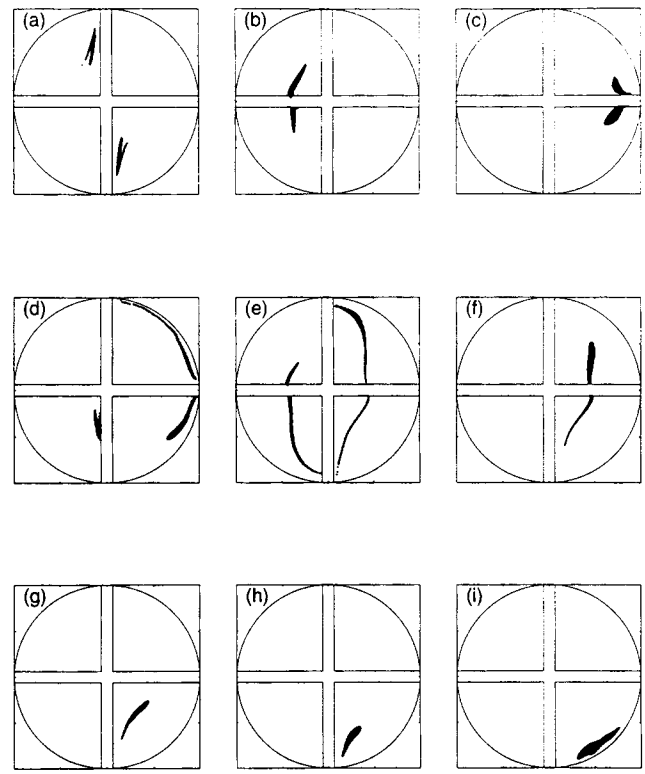

Figure 10. Cross-sectional profiles for 1% tracer mixing in a Kenics mixer in the 180° R-R configuration after 2 elements for each injection location in Figure 2a.

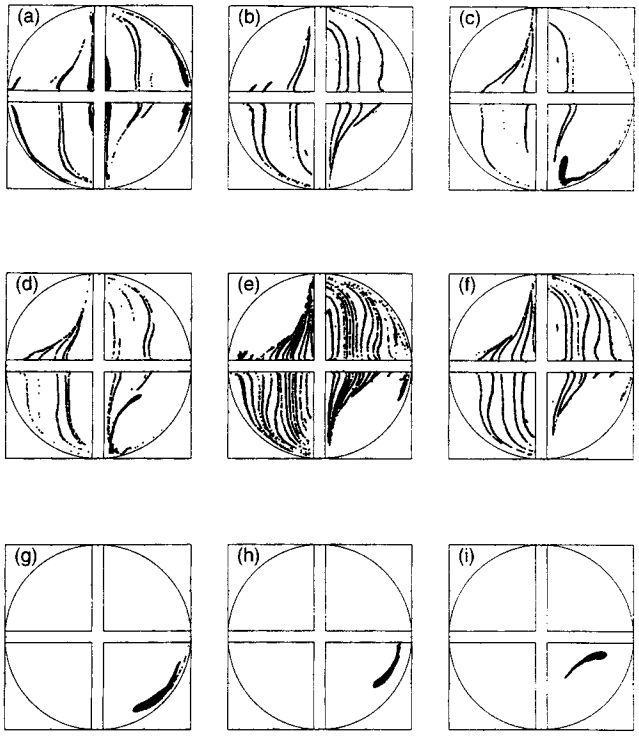

Figure 11. Cross-sectional profiles for 1% tracer mixing in a Kenics mixer in the 180° R-R configuration after 6 elements for each injection location in Figure 2a.

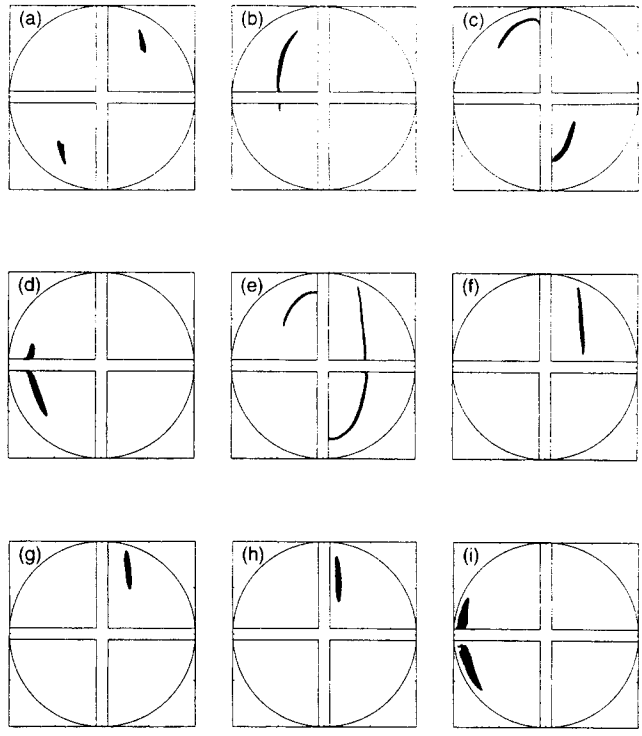

Figure 13. Cross-sectional profiles for 1% tracer mixing in a Kenics mixer in the 120° R-L configuration after 2 elements for each injection location in Figure 2a.

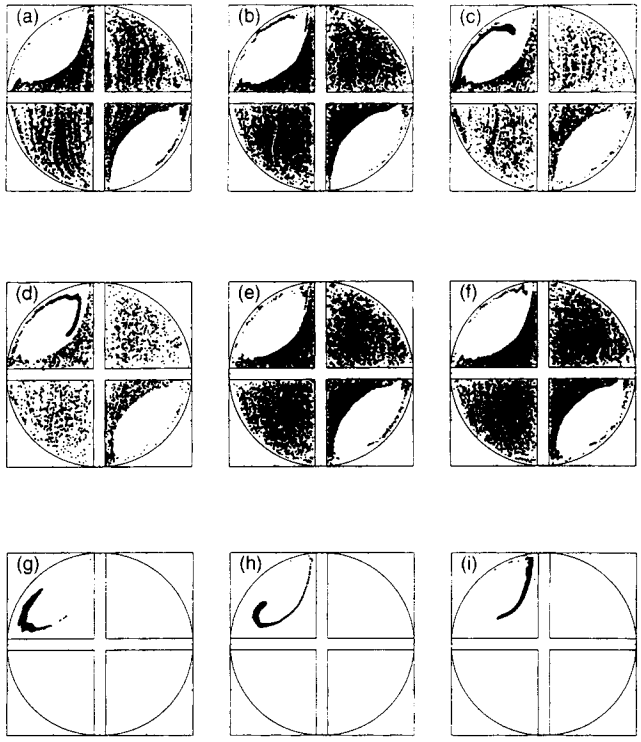

Figure 12. Cross-sectional profiles for 1% tracer mixing in a Kenics mixer in the 180° R-R configuration after 12 elements for each injection location in Figure 2a.

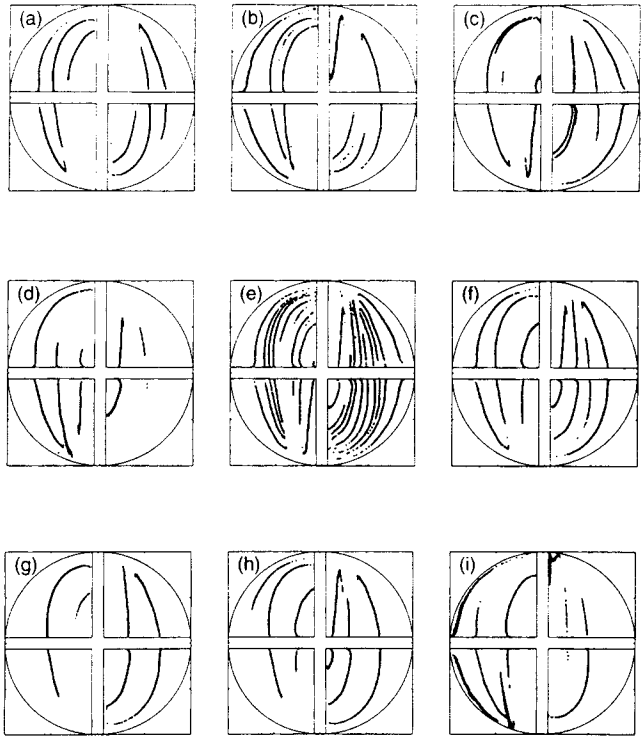

Figure 14. Cross-sectional profiles for 1% tracer mixing in a Kenics mixer in the 120° R-L configuration after 6 elements for each injection location in Figure 2a.

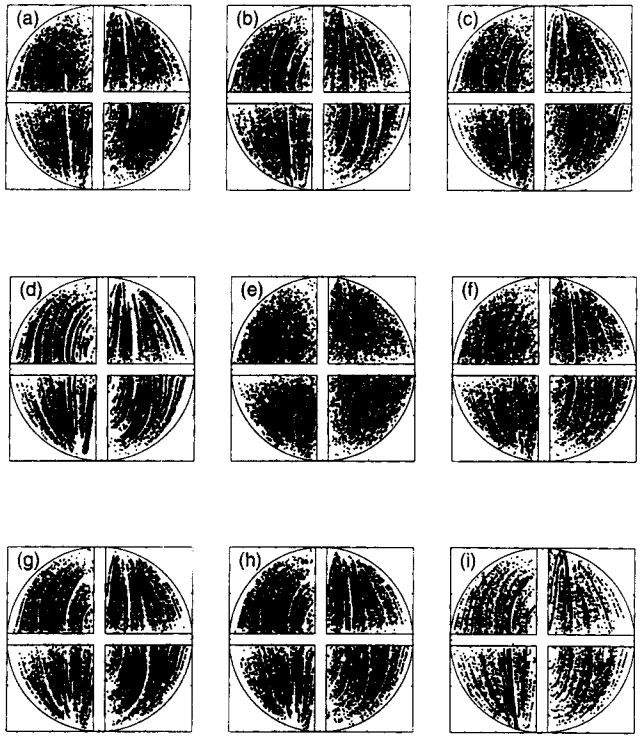

Figure 15. Cross-sectional profiles for 1% tracer mixing in a Kenics mixer in the 120° R-L configuration after 12 elements for each injection location in Figure 2a.

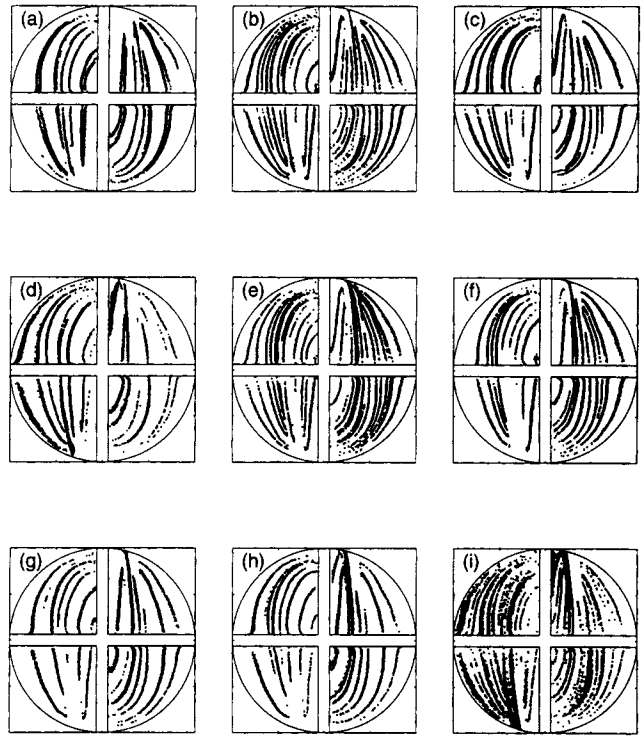

Figure 17. Cross-sectional profiles for 10% tracer mixing in a Kenics mixer in the 120° R-L configuration after 6 elements for each injection location in Figure 2a.

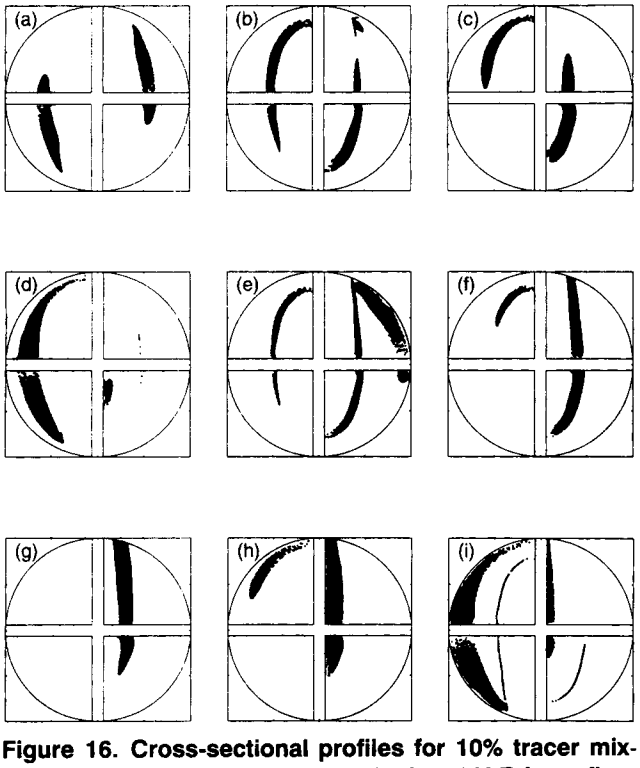

Figure 16. Cross-sectional profiles for 10% tracer mixing in a Kenics mixer in the 120° R-L configuration after 2 elements for each injection location in Figure 2a.

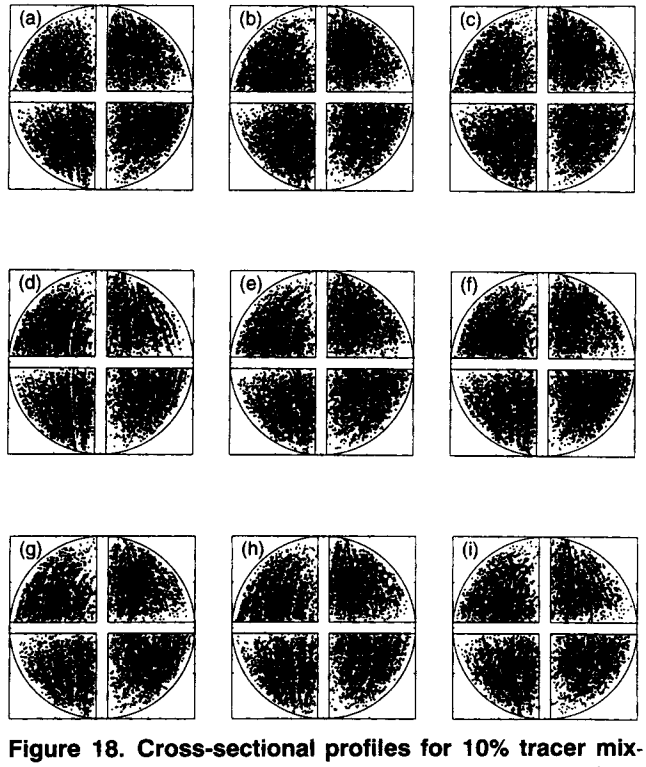

Figure 18. Cross-sectional profiles for 10% tracer mixing in a Kenics mixer in the 120° R-L configuration after 12 elements for each injection location in Figure 2a.

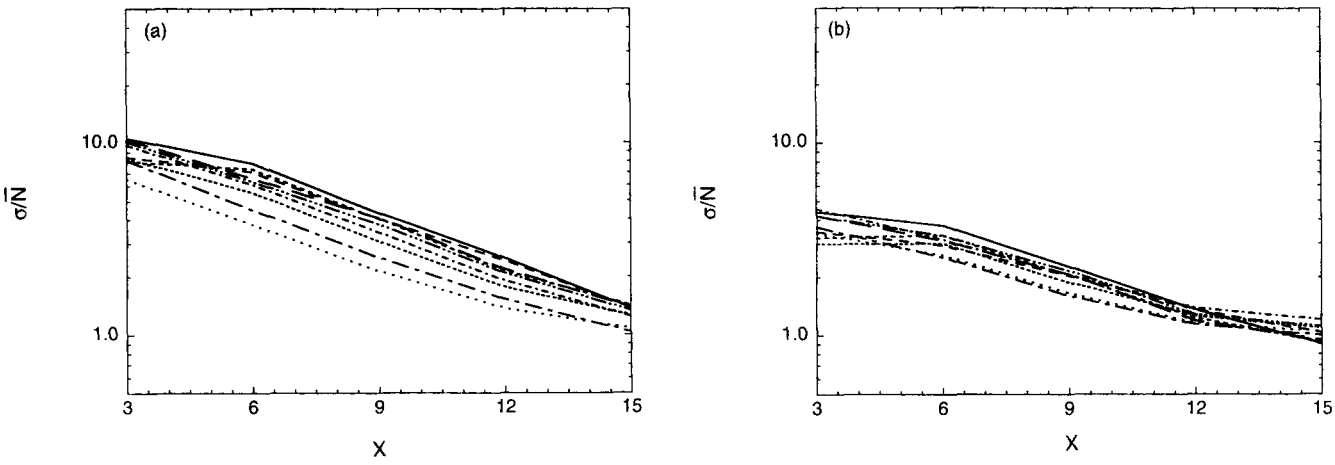

Figure 19. Variation coefficient vs. normalized axial position X and injection position for a Kenics mixer in the 180° R-L configuration.

(a) 1% tracer, (b) 10% tracer. Injection position: —— *a*; —— *b*; --- *c*; ----- *d*; ------ *e*; —·— *f*; —·-·- *g*; —·—·— *h*; ----- *i*.

the cross sections in Figures 3–8), it is clear that the number of elements required to reach a given variation coefficient will depend on the chosen injection location. For example, for a 1% tracer injection, the variation coefficient curve for injection position *a* is shifted to the right of the curve for injection position *f* by $X \approx 4$, indicating that an extra 2 to 3 mixer elements are required to achieve the same variation coefficient. The maximum spread of the variation coefficient curves is $X \approx 6$ (four elements) for the 1% tracer case, and $X \approx 3$ (two elements) for the 10% tracer case. In both cases, the injection positions *e*, *f* and *i* require the fewest elements to achieve a target variation coefficient.

Variation coefficient curves for 1% tracer injection in the alternative 180° R-R geometry are shown in Figure 20. Unlike the standard 180° R-L case, the variation coefficient curves for the 180° R-R case are not parallel, and different rates of mixing are obtained for different injection locations. The behavior of the variation coefficient corresponds to the trends that were visually evident in Figures 10–12. The variation coefficient decreases most rapidly for injection locations in the chaotic portion of the flow (*a*, *b*, *e*, and *f*), and these curves are all essentially parallel and lead to the same mixing rate. However, the asymptotic value of variation coefficient reached at $X = 15$ is higher in the 180° R-R case than in the 180° R-L case due to the presence of the segregated regions that do not contain any tracer. For injection locations that are inside or partially inside the segregated, regular regions of the flow (positions *c*, *d*, *g*, *h*, and *i*), the variation coefficient decreases only slightly as a function of axial position since the tracer dispersion remains extremely nonuniform.

Finally, the variation coefficient results for the 120° R-L geometry are plotted in Figure 21a for 1% tracer injection and Figure 21b for 10% tracer injection. The variation coefficient results in this case closely resemble the standard 180° R-L case. For each tracer amount, the curves are once again essentially parallel, indicating that each injection location leads to the same rate of reduction in variation coefficient. The asymptotic level reached by the variation coefficient curves is the same as for the 180° R-L case, limited by the resolution of the computation since no segregated regions are present in the flow.

One difference between the 120° R-L case and the 180° R-L case is the rate of reduction in variation coefficient achieved in each geometry. The average *B* values ($\bar{B}$) for 1 % and 10% tracer injection in the 120° R-L case are 0.248 and 0.153, respectively, compared to 0.167 and 0.116 for the 180° R-L case. Variation coefficient curves for injection position *a* in each geometry are plotted together in Figure 22. From this side-by-side comparison, it is clear that the 120° R-L geometry leads to more rapid mixing per axial distance than the standard geometry.

In addition to overall mixing per unit length, another concern when comparing mixer configurations is the energy input required to produce the desired mixing. For a static mixer, the pressure drop through the mixer provides a direct measure of the energy required to generate mixing in the system. Using $\bar{B}$ for each mixer as a quantitative measure of mixing performance, a mixing efficiency ϕ can be computed by nor-

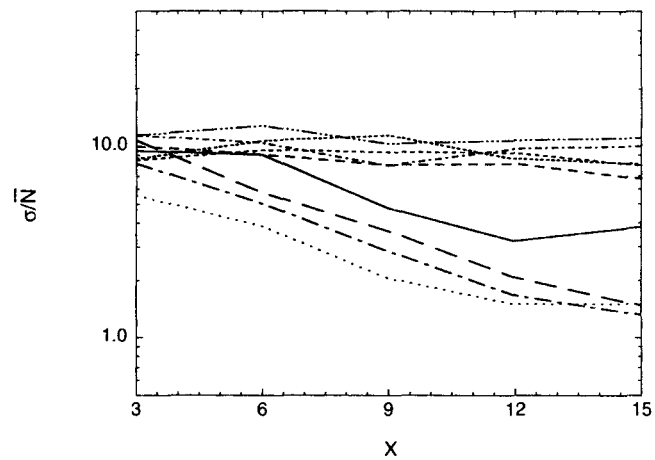

Figure 20. Variation coefficient for a 1% tracer injection vs. normalized axial position X and injection position for a Kenics mixer in the 180° R-R configuration.

Injection position: —— *a*; —— *b*; --- *c*; ----- *d*; ------ *e*; —·— *f*; —·-·- *g*; —·—·— *h*; ----- *i*.

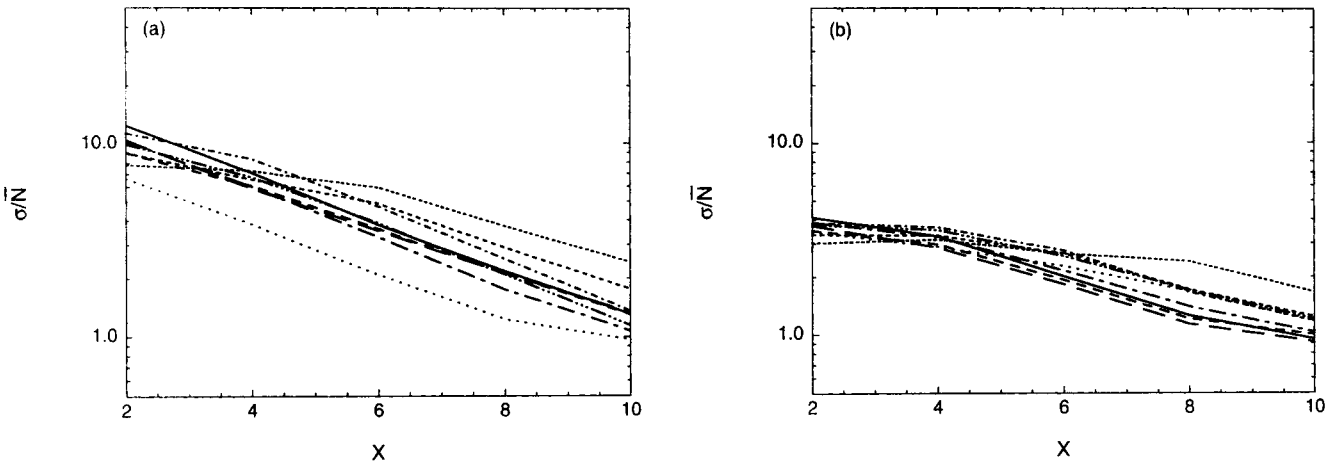

Figure 21. Variation coefficient vs. normalized axial position X and injection position for a Kenics mixer in the 120° R-L configuration.

(a) 1% tracer; (b) 10% tracer. Injection position: —— *a*; —— *b*; --- *c*; ---- *d*; ----- *e*; —·— *f*; —··— *g*; —···— *h*; ····· *i*.

malizing $\bar{B}$ by the mixer pressure drop per unit length. The pressure drop for the 120° R-L and 180° R-L geometries was obtained from CFD computations as 0.618 Pa/cm and 0.586 Pa/cm, respectively (previous results have shown a close agreement between computed pressure drop and experimental data over a broad range of flow velocities in the 180° R-L Kenics geometry (Hobbs and Muzzio, 1997a). Therefore, ϕ values of the 120° R-L mixer are 0.401 and 0.248 for 1% and 10% tracer injections, respectively, and 0.285 and 0.198 for 1% and 10% tracer injections in the 180° R-L mixer. Based on the relative ϕ values for the two geometries, the 120° R-L mixer is 25–40% more energy efficient than the standard Kenics geometry. A similar 40% improvement in efficiency was previously obtained using stretching rates to quantify mixer performance (Hobbs et al., 1997b). The close agreement of these two different approaches indicates that both methods can be employed to provide consistent, complementary information about mixing processes. Computation of the variation coefficient provides a more direct analog to typical experimental approaches, while tracking stretching and the use of other dynamical systems techniques provides additional insight into structures such as periodic points and manifolds that affect mixing in the flow.

Conclusions

The mixing performance of the Kenics static mixer and two variations on the standard mixer geometry was investigated using tracer mixing simulations and computations of the variation coefficient. Nine different tracer injection locations were investigated, as well as 1% and 10% injections of tracer. Cross-sectional slices from the mixing simulations supply visual, qualitative information about the development of partially mixed structures for each flow condition. Profiles of variation coefficient vs. axial position provide quantitative information about mixing rate and efficiency.

All injection locations in the standard 180° R-L Kenics mixer give essentially identical rates of reduction in the variation coefficient. In one sense, this implies that injection location is unimportant if a sufficiently long mixer is available, since all injection locations will eventually produce a mixture that has the desired level of homogeneity. On the other hand, the location of the initial injection has a large effect on the spread of tracer over the first few mixer elements, and a corresponding trend in variation coefficient profiles is observed. The number of mixer elements required to produce a target variation coefficient may differ by up to four elements depending on the injection location. For a typical industrial application using a 6- or 12-element Kenics mixer, this dependence on inlet conditions could have a significant impact on product quality. The injection locations *e*, *f*, and *i* lie along the unstable manifolds of hyperbolic periodic points that produce highly stretched regions in the flow, and these injection locations produce the most effective tracer dispersion over the first few mixer elements.

Similar effects of injection location were evident for the 120° R-L geometry. Results for rate of reduction of variation coefficient normalized by pressure drop indicate that the 120° R-L geometry is 25–40% more energy efficient than the stan-

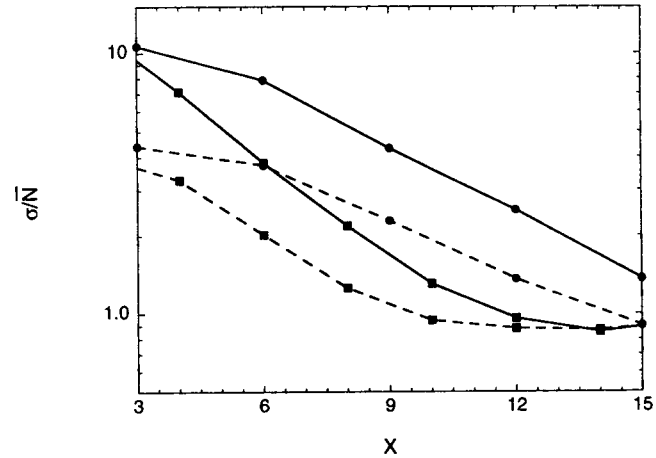

Figure 22. Variation coefficient vs. normalized axial position X for tracer injection position (a).

—●— 180° R-L, 1% tracer; -·●·- 180° R-L, 10% tracer; —■— 120° R-L, 1% tracer; -·■·- 120° R-L, 10% tracer.

dard 180° R-L configuration. Quantitatively similar results for improved mixer performance in the 120° R-L configuration were obtained using an energy-efficiency measure based on stretching rates (Hobbs et al., 1997b). Tracer mixing cross sections for the alternative 180° R-R geometry illustrate the presence of segregated regions in this flow, which have been previously observed (Hobbs et al., 1997a). Variation coefficient calculations quantitatively capture the poor mixing performance of this system relative to the standard Kenics geometry.

Coupled with CFD methods to obtain velocity fields, Lagrangian tracer-tracking computations provide a viable means of simulating mixing processes in industrial flows. The computation of traditional mixing measures such as the variation coefficient provides a tangible and quantitative description of mixing behavior that can be compared with existing experimental data to help to tie together the simulation and experimental approaches. Lagrangian tracking computations can be extended to other properties of interest (such as the stretching or curvature of material lines) that provide a useful description of mixing behavior in the Kenics flow. Such simulations provide a practical means to evaluate different mixer geometries and mixing scenarios computationally before undertaking costly experimental investigation. The Lagrangian tracking tools that have been developed to analyze the Kenics mixer could also be applied to other types of static mixers, or to other properties of interest in mixing equipment, such as striation thickness distributions, or chemical reactions. Work in these areas is in progress in our laboratory and will be presented in future communications.

Acknowledgments

This work was supported by awards from NSF (CTS 94-14460), from 3M, and from Dupont to F.J.M. D.M.H. is grateful to Merck and Co., Inc. for support during the performance of this work.

Notation

D = mixer diameter
L = axial length of a single mixer element
R = mixer radius
$v(x)$ = particle velocity as a function of position
x = vector of particle position (x, y, z)

Literature Cited

Allocca, P. T., "Mixing Efficiency of Static Mixing Units in Laminar Flow," *Fiber Prod.*, **8**(82), 12 (1982).

Danckwerts, P. V., "The Definition and Measurement of Some Characteristics of Mixtures," *Appl. Sci. Res.*, **A3**, 279 (1952).

Fan, L. T., S. J. Chen, and C. A. Watson, "Solids Mixing," *Ind. Eng. Chem.*, **62**(7), 53–69 (1970).

Godfrey, J. C., "Static Mixers," Mixing in the Process Industries, N. Harnby, M. F. Edwards, and A. W. Nienow, eds., Butterworth-Heinmann, Oxford, p. 225 (1992).

Hobbs, D. M., and F. J. Muzzio, "The Kenics Static Mixer: A Three-Dimensional Chaotic Flow," *Chem. Eng. J*, (1997a).

Hobbs, D. M. and F. J. Muzzio, "Optimization of a Static Mixer Using Dynamical Systems Techniques," *Chem. Eng. Sci.*, submitted (1997b).

Hobbs, D. M., P. D. Swanson, and F. J. Muzzio, "Numerical Characterization of Low Reynolds Number Flow in the Kenics Static Mixer," *Chem. Eng. Sci.* (1997a).

Hobbs, D. M., M. M. Alvarez, and F. J. Muzzio, "Mixing in Globally Chaotic Flows: A Self-Similar Process," *Fractals*, (to appear) (1997b).

Leong, C. W. and J. M. Ottino, "Experiments on mixing due to chaotic advection in a cavity," *J. Fluid Mech.*, **209**, 463–499 (1989).

Middleman, S., *Fundamentals of Polymer Processing*, McGraw-Hill, New York (1977).

Nauman, E. B., "On residence time and trajectory calculations in motionless mixers," *Chem. Eng. J.*, **47**, 141 (1991).

Pahl, M. H., and E. Muschelknautz, "Static Mixers and Their Applications," *Int. Chem. Eng.*, **22**(2), 197 (1982).

Paul, E. L., "Design and Scaleup of an Anchorage-dependent Mammalian Cell Bioreactor," *Ann. NY Acad. Sci.*, **589**, 642 (1990).

Press, W. H., B. P. Flannery, S. A. Teukolsky, and W. T. Vetterling, *Numerical Recipes (The Art of Scientific Computing)*, Cambridge Univ. Press, Cambridge, England (1986).

Swanson, P. D., and J. M. Ottino, "A Comparative Computational and Experimental Study of Chaotic Mixing of Viscous Fluids," *J. Fluid Mech.*, **213**, 227 (1990).

Manuscript received Apr. 14, 1997, and revision received July 23, 1997.